Comparison of planar shear flow and planar elongational flow for systems of small molecules

M. L. Matin and P. J. Daivis
Department of Applied Physics, RMIT, GPO Box 2476V, Melbourne, Victoria 3001, Australia

B. D. Todd
Centre for Molecular Simulation and School of Information Technology, Swinburne University of Technology, P.O. Box 218, Hawthorn, Victoria 3122, Australia

(Received 10 July 2000; accepted 28 August 2000)

We use nonequilibrium molecular dynamics to simulate steady state planar shear flow and planar elongational flow of fluids of small molecules at constant volume and temperature. The systems studied are Lennard–Jones diatomic molecules (chlorine), and a series of linear Lennard–Jones molecules with one, two, and four sites. In our simulations of planar elongational flow, we employ Kraynik–Reinelt periodic boundary conditions, which allow us to obtain precise values of the steady state planar elongational viscosity. We validate our application of Kraynik–Reinelt periodic boundary conditions by comparing the zero strain rate shear and elongational viscosities. The results show that the elongational viscosity is proportional to the shear viscosity in the zero strain rate limit, as expected. The viscosity, pressure, and internal energy of the atomic Lennard–Jones fluid show exactly the same behavior for the two types of flow when both sets of results are plotted against the second scalar invariant of the strain rate tensor. The results for the diatomic and four-site molecules show differences in the pressure, energy, and viscosity outside the Newtonian regime when plotted against the second scalar invariant of the strain rate tensor. The differences in the properties in the nonlinear regime increase with both strain rate and molecular length. © *2000 American Institute of Physics.* [S0021-9606(00)50144-5]

I. INTRODUCTION

The rheological properties of molecular and polymeric fluids have a direct impact on many manufacturing processes such as blow-forming, injection molding, and sheet casting. The flows occurring during these processes are complicated and will usually involve some combination of planar Couette flow (PCF), planar elongational flow (PEF), and biaxial/uniaxial stretching flow (BSF/USF). Control of these processes demands an adequate understanding of rheological properties, and preferably, an ability to predict rheological behavior from the molecular characteristics of the materials in question.

Our current understanding of the molecular basis of rheology is based almost entirely on models that involve major assumptions. Discriminating tests of these assumptions can only be performed at the molecular level, so there is a need for direct investigations of the molecular processes that determine rheological behavior. Nonequilibrium molecular dynamics (NEMD) is an ideal tool for the investigation of the microscopic detail underlying the macroscopic properties of fluids, but some questions of technique, validity, and efficiency need to be addressed before NEMD can confidently be used to test theories of polymer rheology or to directly predict the rheological properties of polymeric fluids.

Although the equations of motion and the corresponding periodic boundary conditions (PBCs) for the simulation of shear flow are now well known and validated, the simulation of elongational flow has been more difficult. Early PEF simulations involved contracting the simulation cell in one of the directions parallel to the (orthogonal) periodic boundaries while expanding it in the perpendicular direction, so as to keep the volume constant. For simulations of systems with short-ranged interactions the minimum image convention imposes a limit on the minimum simulation system dimensions, and this leads to a limitation on the length of the simulation, which may prevent the attainment of a steady state before the end of the simulation. Several different techniques have been proposed as solutions to this problem, but the most successful approach to date is to use the temporally and spatially periodic boundary conditions devised by Kraynik and Reinelt.[1] These have been applied to nonequilibrium molecular dynamics simulations of elongational flow of atomic fluids by Todd and Daivis[2–4] and also by Baranyai and Cummings.[5] The Kraynik–Reinelt periodic boundary conditions allow simulations of planar elongational flow of unlimited duration to be performed. This eliminates the difficulties of extrapolation of a transient response into the steady state or the zero frequency extrapolations that were necessary in previous methods. However, the K-R PBCs cannot be used for uniaxial or biaxial elongational flow. In this case, the oscillatory elongational flow algorithm, with zero frequency extrapolation[6,7] is a viable alternative. The transient behavior of a model polymer melt in uniaxial elongational flow has recently been studied by both experimental and computer simulation methods by Kroger, Luap, and Muller.[8]

Only a few comprehensive comparisons of shear and elongational flow simulations of atomic fluids have previ-

ously been performed.[9–11] The main conclusions to be reached are that the ratio of elongational to shear viscosity approaches the expected value in the zero strain rate limit, and that the strain rate dependence of the shear and planar elongational viscosities fall on a universal curve when plotted as a function of the second scalar invariant of the strain rate tensor. The only existing NEMD data for the steady state elongational viscosity of a molecular fluid were obtained for chlorine,[12] but the results were not conclusive. No systematic study of the effect of molecular size on the comparison between shear and elongational rheology of molecular fluids has previously been published.

In this paper, we investigate the shear and elongational strain rate dependence of several properties including the viscosity, pressure, and internal energy for a variety of fluids. To validate our technique, we present results for a simple model of liquid chlorine that can be compared to previous work. We also present results for monatomic and two- and four-site Lennard–Jones chain molecules to show the effect of molecular size on the rheological behavior.

II. MOLECULAR MODELS

The atomic fluid studied has an interaction potential given by the truncated and shifted Lennard–Jones potential energy function, i.e.,

$$\phi(r_{ij})=4\epsilon\left[\left(\frac{\sigma}{r_{ij}}\right)^{12}-\left(\frac{\sigma}{r_{ij}}\right)^{6}\right]-\phi_c, \tag{1}$$

where r_{ij} is the interatomic separation, ϵ is the potential well depth, and σ is the value of r_{ij} at which the unshifted potential is zero. The shift ϕ_c is the value of the unshifted potential at the cutoff $r_{ij}=r_c$, and is introduced to eliminate the discontinuity in the potential.

We used the same molecular model for our simulations of liquid chlorine as the one used by Evans, Edberg, and Morriss[13] and Hounkonnou, Pierleoni, and Ryckaert[12] to allow a direct comparison of our results with previous work. This model represents chlorine as a diatomic Lennard–Jones molecule with $r_c=2.5\sigma$ and a fixed bond length of 0.63σ. The Lennard–Jones potential parameters quoted by the above authors for an adequate representation of the properties of chlorine are: $\sigma=3.332$ Å and $\epsilon/k_B=178.3$.

The molecular model that we have chosen to represent chain molecules is the Lennard–Jones chain model. Each molecule in this model consists of n sites of equal mass $m_{i\alpha}$ interacting via a truncated and shifted LJ interaction ($r_c=2^{1/6}\sigma$), joined by rigidly constrained bonds of length $l=\sigma$. An LJ potential with this truncation point is often known as the WCA[14] potential, and results in purely repulsive interactions. LJ interactions can occur between any two different sites except those connected by a bond. The equilibrium phase behavior of a model that is identical apart from the choice of cutoff distance r_c has been studied by Johnson, Muller, and Gubbins.[15]

Brownian dynamics simulations of elongational flow for a single Kramers model molecule (freely jointed chain with no excluded volume) have been reported by Liu.[16] In the terminology of Bird *et al.*[17] our model is a bead-rod model with excluded volume. Another frequently studied model is the bead-spring model, employing either harmonic or finitely extensible nonlinear elastic (FENE) spring potentials between beads. NEMD studies of the shear rheology of FENE chain model molecules have been reported by Kroger, Loose, and Hess.[18]

In the remainder of this paper we express all quantities in terms of atomic reduced units in which the reduction parameters are the Lennard–Jones interaction site parameters ϵ and σ and the mass, $m_{i\alpha}$, of interaction site α on molecule i. In our simulations all of the $m_{i\alpha}$ are equal. In terms of the corresponding quantities in real units, the reduced temperature T^* is given by $T^*=k_BT/\epsilon$, the density by $\rho^*=\rho\sigma^3$, the pressure by $p^*=p(\sigma^3/\epsilon)$, the energy by $E^*=E/\epsilon$, and time by $t^*=t/(\sigma(m/\epsilon)^{1/2})$. Reduced strain rates are given by, e.g., $\dot\gamma^*=\dot\gamma\sigma(m/\epsilon)^{1/2}$. The asterisk denoting reduced quantities will be dropped from here on.

III. EQUATIONS OF MOTION

The equations of motion for nonequilibrium molecular dynamics simulations of homogeneous flows of atomic fluids have been discussed before[19,20] and are given by

$$\dot{\mathbf{r}}_i=\frac{\mathbf{p}_i}{m_i}+\mathbf{r}_i\cdot\nabla\mathbf{u}, \tag{2}$$

$$\dot{\mathbf{p}}_i=\mathbf{F}_i-\mathbf{p}_i\cdot\nabla\mathbf{u}-\zeta_A\mathbf{p}_i, \tag{3}$$

where $\mathbf{r}_i$ are the atomic positions and $\mathbf{p}_i$ are the atomic peculiar momenta (i.e., the thermal components of the atomic momenta, as defined by the first equation). $\mathbf{F}_i$ is the total force on atom i due to all other atoms. The velocity gradient tensor $\nabla\mathbf{u}$ for a combination of shear flow and planar elongational flow is given by

$$\nabla\mathbf{u}=\begin{pmatrix}\dot\epsilon & 0 & 0\\ \dot\gamma & -\dot\epsilon & 0\\ 0 & 0 & 0\end{pmatrix}. \tag{4}$$

In this paper, we study only the cases where $\dot\gamma=0$ (planar elongational flow) or $\dot\epsilon=0$ (planar shear flow).

The coefficient ζ_A is chosen so as to fix the kinetic temperature, which is defined as

$$T_A=\frac{1}{k_Bf}\sum_{i=1}^{N}\frac{\mathbf{p}_i^2}{m_i}. \tag{5}$$

Several algorithms are available for this purpose.[20] We use the value of ζ_A that results from the application of Gauss' principle of least constraint to the imposition of constant kinetic temperature:

$$\zeta_A=\frac{\sum_{i=1}^{N}(\mathbf{F}_i\cdot\mathbf{p}_i-\mathbf{p}_i\cdot\nabla\mathbf{u}\cdot\mathbf{p}_i)}{\sum_{i=1}^{N}\mathbf{p}_i^2}. \tag{6}$$

In our simulations of molecular fluids, we use the molecular version of the SLLOD equations of motion given by

$$\dot{\mathbf{r}}_{i\alpha}=\frac{\mathbf{p}_{i\alpha}}{m_{i\alpha}}+\mathbf{r}_i\cdot\nabla\mathbf{u}, \tag{7}$$

$$\dot{\mathbf{p}}_{i\alpha}=\mathbf{F}_{i\alpha}^{\mathrm{LJ}}+\mathbf{F}_{i\alpha}^{C}-\frac{m_{i\alpha}}{M_i}\mathbf{p}_i\cdot\nabla\mathbf{u}-\zeta_M\frac{m_{i\alpha}}{M_i}\mathbf{p}_i, \tag{8}$$

where $\mathbf{r}_{i\alpha}$ and $\mathbf{p}_{i\alpha}$ represent the position and thermal momentum of site α of molecule i, $\mathbf{r}_i$ represents the position of the center-of-mass of molecule i, $m_{i\alpha}$ is the mass of site $i\alpha$, $\mathbf{F}_{i\alpha}^{\mathrm{LJ}}$ represents the sum of all LJ type forces on site α of molecule i, and $\mathbf{F}_{i\alpha}^{C}$ represents the sum of all bond length constraint forces on site α of molecule i. ζ_M is the thermostat multiplier, given by

$$\zeta_M=\frac{\Sigma_{i=1}^{N}1/M_i\,(\mathbf{F}_i\cdot\mathbf{p}_i-\mathbf{p}_i\cdot\nabla\mathbf{u}\cdot\mathbf{p}_i)}{\Sigma_{i=1}^{N}1/M_i\,\mathbf{p}_i^2}, \tag{9}$$

where $\mathbf{p}_i=\Sigma\mathbf{p}_{i\alpha}$ represents the center of mass momentum of molecule i and M_i is the mass of molecule i. This expression for ζ_M is similar to Eq. (6) and is also derived from Gauss' principle of least constraint, but acts to keep the molecular center-of-mass kinetic temperature T_M constant, rather than the atomic or site temperature. Here we define T_M by

$$T_M=\frac{1}{k_B f}\sum_{i=1}^{N}\frac{\mathbf{p}_i^2}{M_i}, \tag{10}$$

where f represents the number of translational center-of-mass degrees of freedom, which depends on the total number of sites and the number of constraints (holonomic and nonholonomic) on the system. This algorithm, including the details of the constraint algorithm, has been discussed previously.[21–23]

Note that in the equations of motion, the same strain rate and thermostat terms are applied to all sites on a given molecule. This means that they only affect the center-of-mass degrees of freedom and cannot interfere with intramolecular degrees of freedom. Alternative forms of the equations of motion can be applied (for example, atomic shear with an atomic thermostat), but they can result in a nonzero antisymmetric stress and artificially enhanced orientational ordering. The combination of center-of-mass molecular shear (or elongation) with a molecular center-of-mass thermostat seems to be the simplest choice that suffers the least from the distortions associated with incorrect assumptions about the streaming velocity. We refer the reader to previous work[24–26] on the subtle but important issues involved in thermostats for molecular fluids. For our current purposes, the above equations of motion will suffice.

When they are solved exactly, the SLLOD equations of motion will conserve the total peculiar momentum of the system if it has been initialized to zero. However, we have recently found that when the SLLOD equations of motion are solved numerically for elongational flow, any small error in the component of the total momentum in the contracting direction (due to unavoidable discretization and finite precision arithmetic errors) can grow exponentially, resulting in catastrophic failure of momentum conservation.[4] This failure in the numerical solution of the equations of motion is easily prevented by initializing the total momentum to zero as usual, and then subtracting any change in the total momentum from the system at each timestep. This is a very small correction, which has no effect on the results except to prevent the exponential growth of the numerical error in the momentum.

IV. SIMULATION DETAILS

Our algorithm for constant (N,V,T_M) simulations of Lennard–Jones chain molecules undergoing shear and elongational flow is based on the Evans, Edberg, and Morriss algorithm,[21–23] which we have substantially modified by including cell code for efficient neighbor list construction and appropriate periodic boundary conditions for elongational flow simulations. The details of our cell neighbor list algorithm for elongational flow simulations will be published separately.

To confirm that our program was producing correct results in both shear and elongational flow, we reproduced previous results for the shear and elongational viscosities of Lennard–Jones monatomic and diatomic liquids (representing argon and chlorine). We compared the results of our shear flow simulations of argon at the triple-point to those of Morriss, Evans, and Hood[27] and compared our planar elongational viscosities of argon with those of Todd and Daivis[6] and Baranyai and Cummings.[11] Very good agreement was found in all cases. Our results could not be directly compared with the recent results of Baranyai and Cummings,[5] due to differences in the definitions of the temperatures that were chosen for thermostating, but we observed that our viscosity values were slightly higher, in agreement with their observations. We do not report the results of the argon triple point simulations here.

This paper contains the results of two sets of simulations. In the first set, we improve upon the planar shear and planar elongational flow results of Evans, Edberg, and Morriss[13] and Hounkonnou, Pierleoni, and Ryckaert[12] for liquid chlorine at a reduced temperature of $T=0.9700$ and reduced site number density $\rho=1.088$. A system size of 864 molecules was required in these simulations, so that the minimum image convention would not be violated in PEF. The reduced bond length was $l=0.630$ and the interaction between sites was a truncated (unshifted) LJ potential with $r_c=2.5$ and $\phi_c=0.0$ in Eq. (1). Our results do not include long-range corrections, as it has been shown[28] that the radial distribution function is distorted under PCF making the calculation of long-range corrections by the usual methods difficult and unreliable.

In the second set of simulations, we studied the effect of increasing the chain length on the shear and elongational strain rate dependence of a variety of properties. A series of three different molecular sizes was studied, consisting of one-, two-, and four-site molecules. The parameters of our Lennard–Jones chains were as follows: the LJ potential was truncated at the minimum, $r_c=2^{1/6}$, and shifted to zero at the truncation point. The system size was 256 molecules and the temperature and site density were $T=1.000$ and $\rho=0.840$, respectively. These parameters remained constant throughout this series of simulations. The state point was chosen to correspond to that previously studied by Kroger, Loose, and Hess[18] and Kremer and Grest[29] in their simulations of FENE

TABLE I. Simulation parameters.

	Chlorine	LJ chain
Number of molecules	864	256
Number of sites	2	1, 2, 4
Bond length	0.63	1.00
LJ cutoff	2.5	$2^{1/6}$
Time step	0.001	0.001
Temperature	0.97	1.00
Density	1.088	0.84

chain dynamics. The elongational and shear strain rates varied between 0.0 and 5.0. We summarize the most important simulation parameters in Table I.

All systems were run for at least 100 reduced time units before collecting data at all strain rates to ensure the attainment of a steady state. This time is equivalent to 431 ps for argon, and 326 ps for chlorine. Runs at low strain rates took longer to reach a steady state, and the lengths of some of the production runs at low strain rates were increased to improve their statistical reliability. A few of the elongation runs at high strain rates required smaller time steps but the total time for the production stage was kept constant regardless of the strain rate. The properties of the system were calculated every 0.025 time units, with these being averaged into ten blocks for the production runs, enabling the calculation of standard errors in the means of all measured properties. All production runs were at least 50 time units in length.

The pressure tensor for the atomic fluid (single interaction site molecules) was calculated using the atomic pressure tensor, given by

$$\mathbf{P}_A V = \sum_{i=1}^{N} \frac{\mathbf{p}_i \mathbf{p}_i}{M_i} - \frac{1}{2} \sum_{i=1}^{N} \sum_{j \neq i}^{N} \mathbf{r}_{ij} \mathbf{F}_{ij}, \tag{11}$$

TABLE II. Viscosity, pressure, and total internal energy—864 chlorine molecules, $T=0.9700$, $\rho=1.088$.

	PCF			PEF		
$\dot{\epsilon}, \dot{\gamma}$	η	p	U	η	p	U
0.00	-	1.31	−9240	-	1.30	−9240
0.035	6.75(0.4)	1.32	−9240	6.71(0.4)	1.35	−9230
0.064	6.50(0.5)	1.34	−9230	6.27(0.3)	1.45	−9200
0.085	6.55(0.3)	1.37	−9220	6.10(0.3)	1.51	−9190
0.113	6.34(0.3)	1.41	−9220	5.72(0.1)	1.64	−9150
0.177	5.91(0.2)	1.52	−9190	5.16(0.2)	1.92	−9070
0.212	5.59(0.2)	1.59	−9160	-	-	-
0.255	5.35(0.1)	1.68	−9140	4.77(0.05)	2.31	−8950
0.354	4.96(0.1)	1.89	−9070	4.39(0.06)	2.92	−8750
0.530	4.44(0.1)	2.34	−8940	3.93(0.05)	4.12	−8320
0.693	-	-	-	3.66(0.04)	5.40	−7860
0.707	4.05(0.07)	2.77	−8780	3.64(0.03)	5.52	−7810
1.061	-	-	-	3.39(0.05)	8.99	−6470
1.195	3.52(0.05)	4.39	−8200	-	-	-
1.386	3.41(0.05)	5.10	−7930	-	-	-
1.591	3.32(0.04)	5.98	−7590	-	-	-
1.626	3.32(0.05)	6.18	−7520	-	-	-
1.810	3.24(0.05)	6.97	−7210	-	-	-
2.121	3.17(0.05)	8.53	−6580	-	-	-

TABLE III. Simulation results—one-site LJ fluid ($T=100$, $\rho=0.840$).

	PCF			PEF		
$\dot{\epsilon}, \dot{\gamma}$	η	p	U	η	p	U
0.00	-	7.86	627	-	7.83	625
0.01	-	-	-	1.92(0.5)	7.85	627
0.02	2.13(0.4)	7.85	626	2.03(0.3)	7.86	627
0.05	2.12(0.2)	7.85	626	2.08(0.3)	7.87	627
0.10	2.21(0.2)	7.87	627	2.04(0.1)	7.89	628
0.20	2.13(0.08)	7.88	628	1.96(0.2)	8.00	633
0.50	1.96(0.1)	8.01	633	1.85(0.06)	8.42	652
1.00	1.86(0.06)	8.41	651	1.71(0.03)	9.55	706
2.00	1.65(0.05)	9.50	703	1.64(0.03)	13.4	908
5.00	-	-	-	2.15(0.04)	39.7	2560

while for all molecular fluids, it was calculated using the expression

$$\mathbf{P}_M V = \sum_{i=1}^{N} \frac{\mathbf{p}_i \mathbf{p}_i}{M_i} - \frac{1}{2} \sum_{i=1}^{N} \sum_{\alpha=1}^{n} \sum_{j \neq i}^{N} \sum_{\beta=1}^{n} \mathbf{r}_{i\alpha j\beta} \mathbf{F}^{\text{inter}}_{i\alpha j\beta}, \tag{12}$$

where, as before, $\mathbf{p}_i$ represents the total peculiar momentum of molecule i, as defined by the equations of motion, and $\mathbf{F}^{\text{inter}}_{i\alpha j\beta}$ represents the intermolecular force on site $i\alpha$ due to site $j\beta$. This definition of the molecular pressure tensor assumes that the molecular peculiar momenta are correctly defined by Eq. (7). The pressures quoted in Tables II–V represent the isotropic part of the pressure tensor, given by $p = 1/3\text{Tr}(\mathbf{P})$.

For our shear flow geometry, defined by Eq. (4) with $\dot{\epsilon} = 0$, the generalized non-Newtonian shear viscosity of a fluid subject to PCF is defined as:

$$\eta_S = -\frac{P_{xy} + P_{yx}}{2\dot{\gamma}}. \tag{13}$$

For planar elongational flow, defined by Eq. (4) with $\dot{\gamma} = 0$, we define a generalized nonlinear elongational viscosity as:

$$\eta_E = \frac{P_{yy} - P_{xx}}{4\dot{\epsilon}}. \tag{14}$$

This definition differs by a factor of $\frac{1}{4}$ from definitions that appear in the rheological literature. Inclusion of this factor ensures that as the strain rate approaches zero, $\eta_S = \eta_E$

TABLE IV. Simulation results—two-site LJ fluid ($T=1.000$, $\rho=0.840$).

	PCF			PEF		
$\dot{\epsilon}, \dot{\gamma}$	η	p	U	η	p	U
0.00	-	6.57	998	-	6.57	999
0.01	2.59(0.9)	6.55	996	3.55(1.0)	6.55	996
0.02	3.15(0.5)	6.56	998	2.96(0.6)	6.55	997
0.05	2.93(0.3)	6.57	998	3.04(0.2)	6.57	1000
0.10	2.97(0.2)	6.57	1000	2.89(0.1)	6.57	1003
0.20	2.82(0.3)	6.60	1010	2.60(0.1)	6.70	1031
0.50	2.46(0.07)	6.79	1040	2.32(0.07)	7.50	1159
1.00	2.19(0.04)	7.46	1160	2.16(0.02)	9.89	1557
2.00	2.00(0.02)	9.69	1540	2.48(0.03)	19.4	3322
5.00	2.49(0.06)	25.0	4740	4.56(0.10)	94.1	22300

TABLE V. Simulation results—four-site LJ fluid ($T=1.000$, $\rho=0.840$).

	PCF			PEF		
$\dot{\epsilon},\dot{\gamma}$	η	p	U	η	p	U
0.00	-	5.85	1750	-	5.83	1760
0.01	3.44(1.0)	5.83	1750	3.67(0.8)	5.82	1750
0.02	4.48(0.5)	5.83	1750	4.20(0.3)	5.83	1760
0.05	4.16(0.3)	5.84	1760	4.29(0.3)	5.81	1770
0.10	3.91(0.1)	5.83	1770	4.02(0.2)	5.85	1810
0.20	3.43(0.2)	5.90	1810	3.82(0.1)	6.14	1970
0.50	2.84(0.06)	6.32	2010	3.46(0.07)	7.95	2820
1.00	2.60(0.06)	7.72	2620	3.84(0.1)	14.4	5950
2.00	2.62(0.06)	12.5	4990	5.70(0.1)	43.6	24 200
5.00	3.94(0.07)	46.6	28 700	-	-	-

$=\eta_0$. A definition of a generalized non-Newtonian viscosity for arbitrary strain rate tensors has been given by Hounkonnou, Pierleoni, and Ryckaert[12] as follows:

$$\eta=-\frac{\mathbf{P}:\mathbf{D}}{\mathbf{D}:\mathbf{D}}, \tag{15}$$

where $\mathbf{D}=(\nabla\mathbf{u}+(\nabla\mathbf{u})^{\mathbf{T}})$ is the symmetric rate of strain tensor (also known as the stretching tensor in the rheological literature). This definition of the viscosity reduces to η_S and η_E as given above when the appropriate strain rate tensors are inserted. Note that our use of the full pressure tensor rather than the excess (nonequilibrium) part alone causes no difficulties, because the equilibrium part of the pressure makes no contribution to either of the generalized viscosities.

The total internal energy was calculated using:

$$U=\sum_{i=1}^{N}\sum_{\alpha=1}^{n}\frac{\mathbf{p}_{i\alpha}^2}{2m_{i\alpha}}+\sum_{i=1}^{N-1}\sum_{\alpha=1}^{n}\sum_{j=i+1}^{N}\sum_{\beta=1}^{n}\phi_{i\alpha j\beta}+\sum_{i=1}^{N}\sum_{\alpha=1}^{n-2}\sum_{\beta=\alpha+2}^{n}\phi_{i\alpha i\beta}, \tag{16}$$

where the first term gives the peculiar kinetic energy, the second term gives the intermolecular potential energy, and the third term gives the intramolecular potential energy. The site indexing scheme used in the expression for the intramolecular potential energy given here is clearly only valid for linear molecules, and the intramolecular term is not needed at all for molecules with less than three sites.

V. RESULTS AND DISCUSSION

We report results for the strain rate dependence of the viscosity, pressure and total internal energy in the various systems studied in Tables II–V. Uncertainties in the viscosities are given in brackets. The uncertainties in the energies and pressures were insignificant.

A reasonable first attempt at a unified description of shear and elongational rheological data can be made by plotting all results as a function of the second scalar invariant, I_2, of the strain rate tensor, as was done by Hounkonnou, Pierleoni, and Ryckaert.[12] The three scalar invariants of the strain rate tensor, I_1, I_2, and I_3, are given by[30]

$$I_1=\mathrm{Tr}(\mathbf{D}),\quad I_2=\mathrm{Tr}(\mathbf{D}\cdot\mathbf{D}),\quad I_3=\mathrm{Tr}(\mathbf{D}\cdot\mathbf{D}\cdot\mathbf{D}). \tag{17}$$

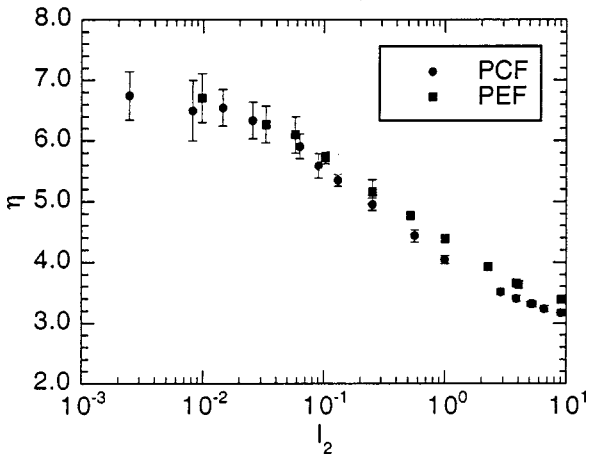

FIG. 1. Viscosity of model chlorine liquid as a function of the second scalar invariant of the strain-rate tensor I_2, for shear and elongational flow, at $T=0.9700$, $\rho=1.088$.

For planar shear and planar elongational flow, the first and third scalar invariants are equal to zero, leaving only the second scalar invariant. The second scalar invariant is related to the strain rate by $I_2=2\dot{\gamma}^2$ for shear flow and $I_2=8\dot{\epsilon}^2$ for planar elongational flow. Physically, I_2 is a measure of the rate of viscous heat dissipation in steady state flow.

First, we will discuss our results for chlorine. Later we consider the Lennard–Jones chains as a series, including the monatomic Lennard–Jones fluid for comparison.

Our results for chlorine cover more than three orders of magnitude, from the Newtonian regime up to $I_2=9.00$. Due to the large number of molecules, and long simulation times, these results have high precision, even in the low strain-rate limit. This allows the Newtonian regime to be seen quite clearly. The viscosity, pressure, and internal energy are plotted in Fig. 1, Fig. 2, and Fig. 3 respectively. Figure 1 shows the expected convergence of the PEF and PCF viscosities to the same value in the zero strain-rate limit. We find a limiting viscosity value of $\eta_0=6.7\pm0.4$, which agrees with the

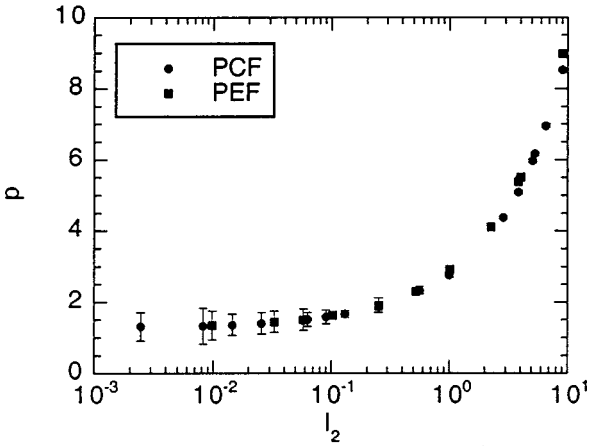

FIG. 2. Pressure of model chlorine liquid as a function of the second scalar invariant of the strain-rate tensor I_2, for shear and elongational flow, at $T=0.9700$, $\rho=1.088$.

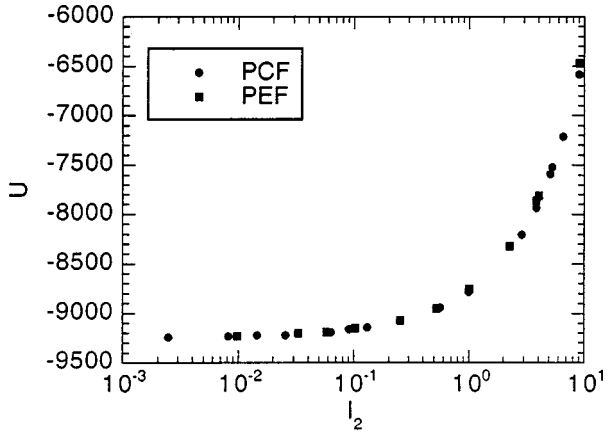

FIG. 3. Internal energy of model chlorine liquid as a function of the second scalar invariant of the strain-rate tensor I_2, for shear and elongational flow, at $T=0.9700$, $\rho=1.088$.

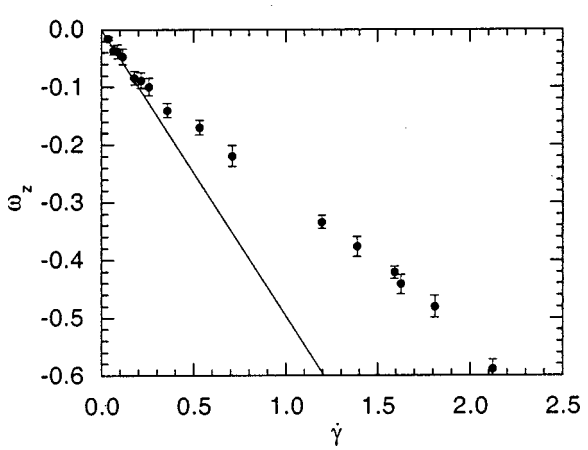

FIG. 4. Molecular spin angular velocity as a function of shear strain rate for liquid chlorine at $T=0.9700$, $\rho=1.088$. The solid line has a slope of -0.5, the result obtained from linear nonequilibrium thermodynamics.

results of Hounkonnou *et al.*,[12] Edberg *et al.*,[13] and Travis *et al.*[24,25] when their results are converted from molecular reduced units to atomic reduced units. (This requires multiplication of their results by a factor of $\sqrt{2}$ to account for the factor of 2 difference between molecular mass and the atomic site mass.) Figure 1 also displays the emerging difference between the two viscosities at higher values of I_2. This difference is significant in our results, but it is obscured by statistical error in the results of Hounkonnou *et al.*[12] For comparison, Table VI shows the results of Hounkonnou *et al.* converted to atomic reduced units alongside our results.

Figure 1, Fig. 2, and Fig. 3 all show that only the lowest three values of I_2 lie clearly inside the Newtonian regime, which ends at $I_2 \approx 0.01$, but they also show that the approximate agreement between these quantities for the two types of flow persists well beyond the end of the Newtonian regime.

We now consider the molecular spin. For diatomic and larger molecules, the equation of change for the spin angular momentum density is given by[24,25]

$$\rho \frac{d\mathbf{S}}{dt} = -\nabla \cdot \mathbf{Q} - 2\mathbf{P}_M^a, \tag{18}$$

where $\mathbf{Q}$ is the couple tensor, which represents the diffusive flow of spin angular momentum and $\mathbf{P}_M^a$ represents the pseudovector dual of the antisymmetric component of the molecular pressure tensor. The couple tensor term is negligible[24] and the linear constitutive equation for $\mathbf{P}_M^a$ can be written as

$$\mathbf{P}_M^a = -\eta_r(\nabla \times \mathbf{u} - 2\omega), \tag{19}$$

TABLE VI. Comparison of our results with HPR (Ref. 12)—liquid chlorine.

I_2	η_S (HPR)	η_E (HPR)	η_S (This work)	η_E (This work)
0.09	5.5(0.3)	-	5.6(0.2)	-
1.00	4.03(0.17)	4.33(0.17)	4.05(0.07)	4.39(0.06)
3.83	3.35(0.11)	3.51(0.08)	3.41(0.05)	3.66(0.04)
9.00	2.94(0.08)	3.30(0.06)	3.17(0.05)	3.39(0.05)

where η_r is the vortex viscosity and ω is the streaming component of the local molecular angular velocity vector. In a steady state, the left hand side of Eq. (18) is equal to zero. Using Eq. (19), this implies that in PCF in the linear regime, we should find

$$\omega_z = -\frac{\dot{\gamma}}{2} \tag{20}$$

at low strain rates. This is observed in the zero strain-rate limit for all systems with more than one site that were studied. The results for chlorine are shown in Fig. 4. Outside the linear regime, the rate of change of shear-induced rotation with increasing strain rate decreases. This is similar to what has been found in simulations of model alkanes,[31–33] where the decrease in the slope of the spin angular velocity graph corresponds to rapidly increasing pressure and saturation of the shear induced order. The value of ω_z at the lowest strain rate was -0.015, and since this simulation ran for 200 reduced time units, each molecule rotated, on average, 0.48 times during the simulation.

In the case of PEF, we have $\nabla \times \mathbf{u} = \mathbf{0}$, and so we expect $\omega = 0$ which is verified for chlorine as shown in Fig. 5. This

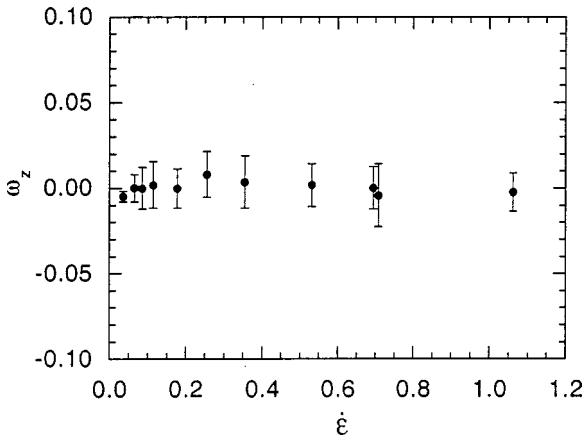

FIG. 5. Molecular spin angular velocity as a function of elongational strain rate for liquid chlorine at $T=0.9700$, $\rho=1.088$.

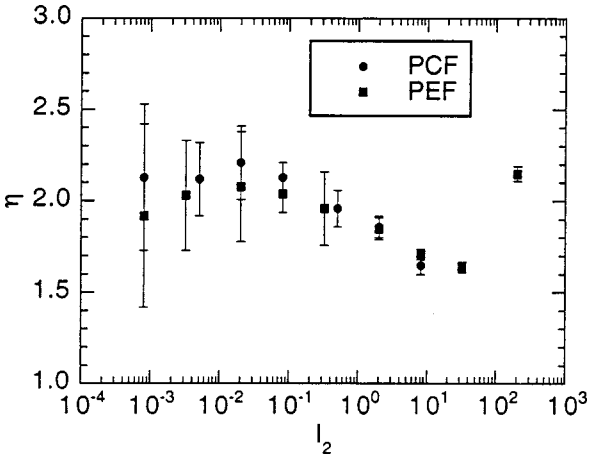

FIG. 6. Viscosity of an atomic LJ liquid as a function of the second scalar invariant of the strain-rate tensor I_2, for shear and elongational flow at $T=1.000$ and $\rho=0.840$.

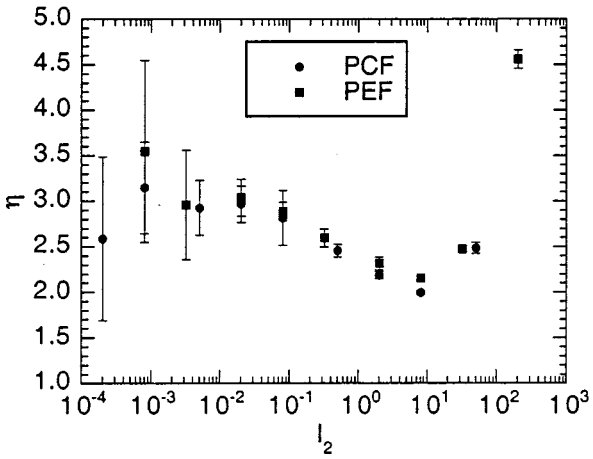

FIG. 7. Viscosity of a two-site LJ tangent chain (i.e., LJ dumbbell) liquid as a function of the second scalar invariant of the strain-rate tensor I_2, for shear and elongational flow at $T=1.000$ and $\rho=0.840$.

is not a trivial result—it indicates that our algorithm, in particular our thermostat, does not apply any unintended torque to the molecules, and can be taken as validating the molecular thermostating approach taken here. This is further supported by the observation that the antisymmetric part of the molecular stress tensor was zero to within uncertainties in the steady state for all of our nonequilibrium simulations.

We now turn to the analysis of the results for Lennard–Jones monatomic and chain fluids.

The viscosity of the monatomic fluid is plotted against I_2 in Fig. 6. The two viscosity curves shown in Fig. 6 converge to a common value as $I_2 \to 0$, giving a limiting zero strain-rate viscosity of 2.1 ± 0.2. The Newtonian region extends to $I_2=0.1$, where we observe the beginning of a shear thinning region. Note that our results for the monatomic fluid extend to higher values of I_2 than were covered in our simulations of liquid chlorine, allowing us to observe the high strain rate regime. Above $I_2=32$ ($\dot{\epsilon}=2.00$ or $\dot{\gamma}=4.00$), shear thickening behavior is observed. This is a common feature in simulations where the density remains constant as the strain rate is increased, and it is accompanied by a dramatic increase in the isotropic pressure. In constant pressure simulations of liquid alkanes, it has been shown that if the volume is allowed to increase, the shear thickening that is observed under constant volume conditions disappears. The disappearance of shear thickening is accompanied by a dramatically reduced first normal stress difference and enhanced molecular spin.

If the rates of heat dissipation at the highest strain rates that we have simulated are converted directly into physical units using the Lennard–Jones parameters; for argon, for example, they are extremely high, and in fact unphysical. However, they are not unrealistic when expressed in reduced units, and we prefer to think of our model molecules as representing appropriately scaled models of molecular fluids for which reduced strain rates of the order of unity are observable in the laboratory. In this sense, the two-site molecules, for example, should be regarded as a dumbbell model for a polymer, with the appropriate mass, energy and distance reduction parameters.

We observed string phases[19] in the PCF simulations of the monatomic LJ fluid at the highest strain rate used, but have not included the data in this paper. Since there was a large gap between the highest and second highest strain rate used in the PCF simulations, the exact value of $\dot{\gamma}$ above which string phases will always be observed is unknown. It has been shown[24,25] that string phases occur when the velocity profile assumed in the equations of motion becomes unstable, and they can be removed by computing, rather than assuming, the streaming velocity profile that is used to calculate the thermal components of the momenta.

The data show that the steady state shear and elongational rheology of this fluid can be described in terms of a single parameter, I_2. Of all the fluids studied in this work, the LJ fluid is the only one that is very well described in this way.

Figures 7 and 8 show the strain-rate dependence of the viscosity for the two- and four-site molecules, respectively. These results show an increase in the difference between the PEF and PCF results as the chain length increases.

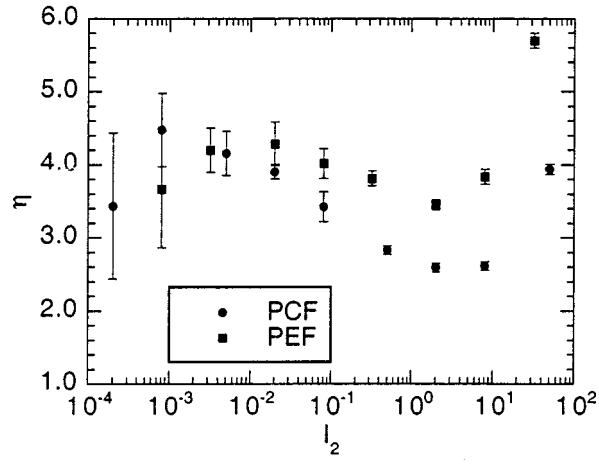

FIG. 8. Viscosity of a four-site LJ tangent chain liquid as a function of the second scalar invariant of the strain-rate tensor I_2, for shear and elongational flow at $T=1.000$ and $\rho=0.840$.

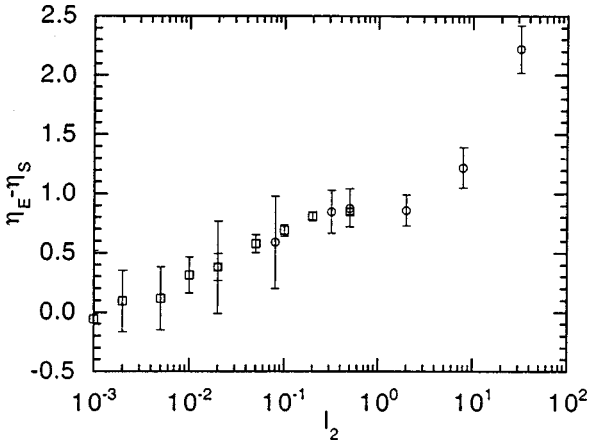

FIG. 9. Difference between elongational and shear viscosities for four-site LJ chains at $T=1.000$ and $\rho=0.840$. Data from previous plots are represented by circles and new data are represented by squares.

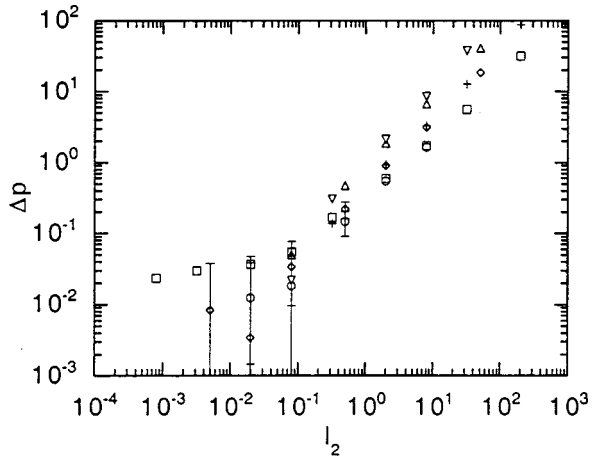

FIG. 10. Isotropic pressure change (compared to equilibrium) for one-, two-, and four-site fluids under shear and elongational flow. Symbols: one-site PCF (circles), PEF (squares); two-site PCF (diamonds), PEF (crosses); four-site PCF (up triangles), PEF (down triangles). Results of power law fits are given in Table VIII.

Extra runs have been done for the four-site system, so that a more detailed plot of the viscosity differences versus I_2 could be made. The results are shown in Fig. 9. The viscosity difference $(\eta_{\mathrm{PEF}}-\eta_{\mathrm{PCF}})$ clearly increases with increasing I_2, but not in a simple way. Three distinct regions are apparent in Fig. 9. At low strain rates, the viscosity difference is zero within uncertainties, and then grows approximately logarithmically until it reaches a plateau value that corresponds to the end of the shear thinning and elongation thinning regions. From there, it appears to grow rapidly again.

Baranyai and Cummings[11] proposed that shear and elongational flows should be equivalent, even in the nonlinear regime, provided that the first normal stress difference, $N_1=P_{yy}-P_{xx}$ in shear flow is zero. This is confirmed by our data, shown in Table VII. It is only for the simple LJ fluid that we find $N_1=0$ within uncertainties, well into the nonlinear regime. In fact, N_1 deviates from zero only for the highest strain rate ($I_2=50$) for the LJ fluid, whereas it begins to deviate from zero for the two- and four-site molecules at approximately the same value of I_2 at which the two viscosities begin to differ significantly.

The absence of first normal stress differences in shear flow is often associated with inelasticity.[30,34–36] On the other hand, the elasticity of a fluid has no effect on the steady state elongational stress of the fluid.[36] Thus the constitutive equation for steady elongational flow is identical to the constitutive equation for inelastic shear flow. Both are described by the Reiner–Rivlin equation, which expresses the stress tensor as

$$\mathbf{P}=p\mathbf{1}+\phi_1(I_2,I_3)\mathbf{D}+\phi_2(I_2,I_3)\mathbf{D}^2. \tag{21}$$

For the flows discussed here, $I_3=0$, giving the result that the stress tensor, and hence the viscosity, will be a function only of the second scalar invariant of the strain rate tensor, as we have found for the monatomic fluid.

The LJ fluid studied here is evidently a good approximation to an inelastic fluid. It is worth noting that a hard sphere fluid is apparently perfectly inelastic in the linear regime at all frequencies.[34] The difference between the behavior of the atomic and molecular fluids found here is consistent with our understanding of the physical mechanisms determining the relaxation of atomic and molecular fluids. The response of an atomic fluid to shear is governed by the elliptical distortion of the radial distribution function, but it is primarily orientational ordering that determines the response of nonspherical molecular fluids to shear flow. The relaxation times, and hence the decay times of the stress autocorrelation functions for these fluids, are markedly different, leading to a primarily inelastic response for the rapidly relaxing atomic fluids and a substantially elastic response in the case of the molecular fluids.

The strain rate dependence of the nonequilibrium pressure and internal energy differences for the one-, two-, and four-site LJ molecules are shown in Fig. 10 and Fig. 11, respectively. In previous work on monatomic fluids[27] and liquid alkanes, it has often been found that the pressure and energy increase in the nonlinear regime due to shear flow are both proportional to $\dot{\gamma}^{3/2}$. Written in terms of I_2, these relationships become

$$\Delta p=p-p_0=AI_2^a, \tag{22}$$

$$\Delta U=U-U_0=BI_2^b, \tag{23}$$

TABLE VII. Normal stress differences—one-, two-, and four-site molecules.

	One-site			Two-site			Four-site		
I_2	N_1	N_2	error	N_1	N_2	error	N_1	N_2	error
0.0002	−0.02	0.01	0.03	0.00	0.00	0.02	0.00	0.01	0.03
0.0008	0.00	0.00	0.03	0.00	−0.01	0.02	0.02	−0.01	0.03
0.005	0.01	0.01	0.03	−0.01	0.00	0.05	0.03	−0.01	0.03
0.02	−0.01	0.00	0.05	0.03	−0.02	0.05	0.14	−0.02	0.05
0.08	0.00	−0.01	0.05	0.16	−0.10	0.10	0.34	−0.14	0.05
0.5	−0.01	−0.04	0.10	0.43	−0.25	0.10	0.85	−0.34	0.05
2	0.04	−0.32	0.14	0.63	−0.50	0.10	1.53	−0.73	0.10
8	0.10	−0.84	0.14	1.18	−1.25	0.10	3.2	−1.87	0.10
50	1.90	−1.05	0.14	4.86	−4.99	0.40	14.94	−8.74	0.50

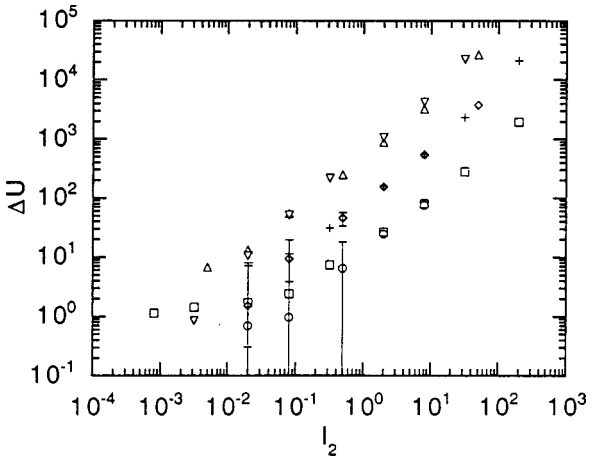

FIG. 11. Internal energy change (compared to equilibrium) for one-, two-, and four-site fluids under shear and elongational flow. Symbols: one-site PCF (circles), PEF (squares); two-site PCF (diamonds), PEF (crosses); four-site PCF (up triangles), PEF (down triangles). Results of power law fits are given in Table VIII.

where $a=b=0.75$. We have fitted power laws of the type given in Eqs. (22) and (23) to the data shown in Fig. 10 and Fig. 11, and the results are given in Table VIII. Table VIII shows that the exponents are all consistently higher than the value of 0.75 found in other work. This may be due to the difference in thermodynamic state points chosen in the different studies. Most of the results for simple LJ fluids have been obtained at the LJ triple point ($T=0.722$, $\rho=0.8442$) which is slightly different from the conditions in these simulations ($T=1.00$, $\rho=0.844$). Our slightly higher temperature presumably results in faster relaxation and enhanced fluidity, in contrast to the typical triple point behavior including the enhanced $t^{3/2}$ tail in the stress autocorrelation function that has often been discussed in the literature. It should also be noted that our exponents, which range from 0.81 up to 1.04 are much closer to the result that would be obtained from the leading term of a power series expansion of Δp in the strain rate, i.e., $\Delta p \propto \dot{\gamma}^2 \propto I_2$. Indeed, recent work by Marcelli *et al.*[37] on shearing fluids with explicit three-body forces show an analytic dependence of pressure on strain rate. It is possible that the $\Delta p \propto \dot{\gamma}^{3/2}$ behavior is only found near the triple point.

Finally, although we do not present the results in detail, we will make a brief comment on the spin angular velocities of the LJ chain molecules. The strain-rate dependence of the molecular spin of the LJ chains was similar to that of chlorine, as discussed earlier. In particular, our simulations verified the expected zero value of the average spin angular velocity in planar elongational flow at all strain rates, and $\omega = -\dot{\gamma}/2$ for planar shear flow in the linear regime.

A general comment should be made regarding the reliability of our results in different strain-rate regimes. The agreement of our results for the limiting Newtonian viscosity of chlorine with those of Hounkonnou *et al.*[12] (computed from the Green–Kubo correlation function expression) indicates that the nonequilibrium and equilibrium molecular dynamics results agree in the zero strain-rate limit. This has also been shown to high precision in simulations of model alkanes.[33] At low strain rates, the approach to the steady state is comparatively slow, and this could be a source of systematic error in the low strain rate region. Yet we observed that results from (usually around 10) consecutive runs in the equilibrated steady state were in good agreement within statistical errors, even at low strain rates. Thus our results are expected to be very reliable in the Newtonian region. The statistical reliability of our data increases as the strain rate increases, and is not a cause for concern outside the Newtonian region, but other issues become significant as the strain rate is increased. Differences in results at high strain rates are obtained when different thermostatting mechanisms are used. We have not used the clearly flawed atomic thermostat for our molecular fluid simulations, but other more subtle differences exist. It has been demonstrated for atomic systems that different results are obtained when the total thermal kinetic energy, or only the thermal kinetic energy computed from the *x*, *y*, or *z* component of the thermal momentum is kept constant.[5] These are not the only possible measures of temperature that could be controlled by a thermostat—the configurational and normal temperatures have also recently been introduced as candidates for a possibly more ''realistic'' measure of temperature under nonequilibrium conditions.[38] These temperatures are all equal at equilibrium, but it remains to be determined which one should be controlled in order to most closely mimic typical experimental nonequilibrium conditions.

VI. CONCLUSION

We have validated the application of Kraynik–Reinelt periodic boundary conditions in nonequilibrium molecular dynamics simulations of molecular fluids and have obtained very precise data for the shear and elongational rheological properties of simple Lennard–Jones fluids and small Lennard–Jones chain fluids. Where comparisons are possible, our results agree with published results obtained by other methods, and we also find agreement with the expected limiting behavior at low strain rates.

The high precision of our results has allowed us to perform a detailed comparison between the shear and elongational flow properties of chlorine and a series of other small molecular fluids.

TABLE VIII. Power law fits for nonequilibrium pressure and energy differences—LJ chain molecules. Uncertainties are given in brackets.

System	*A* (PCF)	*a* (PCF)	*A* (PEF)	*a* (PEF)	*B* (PCF)	*b* (PCF)	*B* (PEF)	*b* (PEF)
one-site	0.28(0.02)	0.87(0.05)	0.37(0.04)	0.81(0.03)	14(2)	0.81(0.07)	13(2)	0.93(0.04)
two-site	0.44(0.02)	0.96(0.02)	0.44(0.02)	0.99(0.02)	83(9)	0.95(0.05)	83(11)	1.01(0.04)
four-site	0.93(0.02)	0.96(0.01)	1.01(0.02)	1.04(0.01)	527(60)	0.95(0.03)	598(37)	1.01(0.02)

We have found that the shear and elongational rheological properties of a simple Lennard–Jones fluid at the state point $T=1.00$, $\rho=0.844$ fall on a universal curve when plotted as a function of the second scalar invariant of the strain rate tensor, I_2, as previously suggested by Ryckaert *et al.* and Baranyai and Cummings. This means that this fluid can be regarded as almost inelastic. In contrast, the molecular fluids all show deviations from this behavior outside the Newtonian region. We find that this is consistent with the suggestion of Baranyai and Cummings that shear and elongational flows are equivalent provided that the first normal stress difference remains close to zero.

The strain-rate dependence of the pressure and energy increases due to shear and elongational flow have also been studied. We find power law behavior with exponents that differ from those found in previous work conducted at lower temperatures, indicating that these exponents are dependent on the thermodynamic state of the system.

The spin of molecules under shear and elongational flow has also been investigated. Our thermostating technique is validated by the finding that the average molecular angular velocity in elongational flow is zero at all strain rates, as expected, and we also observe the expected dependence of the molecular angular velocity on strain rate in shear flow in the linear regime.

ACKNOWLEDGMENTS

The authors would like to thank the CSIRO and the Australian National University for generous grants of time on their supercomputing facilities (NEC SX-4 and VPP300, respectively). This work was supported by the Co-operative Research Centre for Polymers.

[1] A. M. Kraynik and D. A. Reinelt, Int. J. Multiphase Flow **18**, 1045 (1992).
[2] B. D. Todd and P. J. Daivis, Phys. Rev. Lett. **81**, 1118 (1998).
[3] B. D. Todd and P. J. Daivis, Comput. Phys. Commun. **117**, 191 (1999).
[4] B. D. Todd and P. J. Daivis, J. Chem. Phys. **112**, 40 (2000).
[5] A. Baranyai and P. T. Cummings, J. Chem. Phys. **110**, 42 (1999).
[6] B. D. Todd and P. J. Daivis, J. Chem. Phys. **107**, 1617 (1997).
[7] P. J. Daivis and B. D. Todd, Int. J. Thermophys. **19**, 1063 (1998).
[8] M. Kroger, C. Luap, and R. Muller, Macromolecules **30**, 526 (1997).
[9] M. W. Evans and D. M. Heyes, Mol. Phys. **69**, 241 (1990).
[10] C. Pierleoni and J.-P. Ryckaert, Phys. Rev. A **44**, 5314 (1991).
[11] A. Baranyai and P. T. Cummings, J. Chem. Phys. **103**, 10217 (1995).
[12] M. N. Hounkonnou, C. Pierleoni, and J.-P. Ryckaert, J. Chem. Phys. **97**, 9335 (1992).
[13] R. Edberg, D. J. Evans, and G. P. Morriss, Mol. Phys. **62**, 1357 (1987).
[14] J. D. Weeks, D. Chandler, and H. C. Andersen, J. Chem. Phys. **54**, 5237 (1971).
[15] J. K. Johnson, E. A. Muller, and K. E. Gubbins, J. Phys. Chem. **98**, 6413 (1994).
[16] T. W. Liu, J. Chem. Phys. **90**, 5826 (1989).
[17] R. B. Bird, C. F. Curtiss, R. C. Armstrong, and O. Hassager, *Dynamics of Polymeric Liquids* (Wiley, New York, 1987), Vol. 2.
[18] M. Kroger, W. Loose, and S. Hess, J. Rheol. **37**, 1057 (1993).
[19] D. J. Evans and G. P. Morris, *Statistical Mechanics of Nonequilibrium Liquids* (Academic, New York, 1990).
[20] M. P. Allen and D. J. Tildesley, *Computer Simulation of Liquids* (Clarendon, Oxford, 1987).
[21] R. Edberg, D. J. Evans, and G. P. Morriss, J. Chem. Phys. **84**, 6933 (1986).
[22] R. Edberg, G. P. Morriss, and D. J. Evans, J. Chem. Phys. **86**, 4555 (1987).
[23] G. P. Morriss and D. J. Evans, Comput. Phys. Commun. **62**, 267 (1991).
[24] K. P. Travis, P. J. Daivis, and D. J. Evans, J. Chem. Phys. **103**, 1109 (1995).
[25] K. P. Travis, P. J. Daivis, and D. J. Evans, J. Chem. Phys. **103**, 10638 (1995), Erratum: *ibid.* **105**, 3893 (1996).
[26] K. P. Travis and D. J. Evans, Mol. Simul. **17**, 157 (1996).
[27] D. J. Evans, G. P. Morriss, and L. M. Hood, Mol. Phys. **68**, 637 (1989).
[28] D. J. Evans, H. J. M. Hanley, and S. Hess, Phys. Today **37**, 26 (1984).
[29] K. Kremer and G. S. Grest, J. Chem. Phys. **92**, 5057 (1990).
[30] R. B. Bird, R. C. Armstrong, and O. Hassager, *Dynamics of Polymeric Liquids* (Wiley, New York, 1987), Vol. 1.
[31] G. P. Morriss, P. J. Daivis, and D. J. Evans, J. Chem. Phys. **94**, 7420 (1991).
[32] P. J. Daivis, D. J. Evans, and G. P. Morriss, J. Chem. Phys. **97**, 616 (1992).
[33] P. J. Daivis and D. J. Evans, J. Chem. Phys. **100**, 541 (1994).
[34] D. M. Heyes and J. G. Powles, Mol. Phys. **95**, 259 (1998).
[35] W. R. Schowalter, *Mechanics of Non-Newtonian Fluids* (Pergamon, Oxford, 1978).
[36] A. S. Lodge, *Body Tensor Fields in Continuum Mechanics* (Academic, New York, 1974).
[37] G. Marcelli, B. D. Todd, and R. J. Sadus, to be published.
[38] G. Ayton, O. G. Jepps, and D. J. Evans, Mol. Phys. **96**, 915 (1999).